Dynamics of polarons in conjugated polymers: An adaptive time-dependent density-matrix renormalization-group study

Hui Zhao,[1] Yao Yao,[1] Zhong An,[1,2] and Chang-Qin Wu[1]
[1]*Surface Physics Laboratory (National Key Laboratory) and Department of Physics, Fudan University, Shanghai 200433, People's Republic of China*
[2]*College of Physics, Hebei Normal University, Shijiazhuang 050016, People's Republic of China*
(Received 7 March 2008; revised manuscript received 29 April 2008; published 28 July 2008)

The motion of polarons, which serve as charge carriers in conjugated polymers, is of fundamental importance for understanding transport properties of organic optoelectronic devices. We investigate the dynamics of a charged polaron in the presence of both electron-phonon and electron-electron interactions under the influence of an external electric field, which is modeled by the one-dimensional tight-binding Su-Schrieffer-Heeger (SSH) model supplemented with a Hubbard on-site repulsion term. For this many-body dynamical evolution problem, we develop an adaptive time-dependent density matrix renormalization group (*t*-DMRG) method in combination with a Newtonian equation of motion for atomic displacements. Our results show that the velocity of the polaron is suppressed by the on-site Coulomb interaction U. The polaron moves with a supersonic velocity, about four times the sound velocity at the small U limit, and approaches the sound velocity at the large U limit. Furthermore, the dependence of the polaron velocity and the polaron effective mass on the lattice structures are discussed.

DOI: 10.1103/PhysRevB.78.035209 PACS number(s): 72.80.Le, 71.38.Ht, 71.27.+a, 71.15.Pd

I. INTRODUCTION

Conjugated polymers, as quasi-one-dimensional materials, have a property that their lattice structure can be easily distorted due to the strong electron-lattice interactions.[1] As a result, charge injections or photoexcitations will induce self-trapped elementary excitations such as solitons,[2,3] polarons,[4] and neutral polaron excitons. There have been considerable research works devoted to the study of those nonlinear elementary excitations in conjugated polymers.[5] The motivation behind these works stems from the fact that these excitations play an important role in organic optoelectronic devices, including light-emitting diodes, field-effect transistors, photocells, lasers,[6] and so on. For example, in polymer-based light-emitting diodes, it has been generally accepted that injected charge from the metal electrodes deforms the polymer chain to form a polaron, as charge carrier; the polaron transports under the influence of an external electric field. When a positively charged polaron meets a negatively charged one, they will recombine to form a neutral polaron exciton. Then, the exciton decays radiatively to emit a photon. Polymer-based photocells rely on the inverse processes, i.e., charge carriers (charged polarons) generated from the dissociation of polaron excitons. Obviously, in order to improve the performance of these devices, the physics of these processes has to be well understood.

Most of these processes in organic optoelectronic devices, such as the migration of polarons, recombination of oppositely charged polaron pairs, and the dissociation of excitons, are dynamic processes accompanied by both charge and lattice distortions, therefore, a real-time dynamical model revealing both charge motion and lattice evolution will be appropriate. Our previous work on the dynamics of photoexcitations in conjugated polymers also shows that the dynamic characteristics are essentially important to understand the physical phenomena in organic optoelectronic devices.[7] Although the charge transport is largely limited by interchain hopping rather than by intrachain processes in realistic devices, from the theoretical point of view, we focus on the dynamics of charged polarons driven by an external electric field in a single conducting polymer chain. In fact, electronic transport through single conductive molecules (or molecular wires) has been studied intensively theoretically as well as numerically in recent years.[8]

Indeed, based on the one-dimensional tight-binding Su-Schrieffer-Heeger (SSH) Hamiltonian, there have been extensive studies on the polaron dynamics in conjugated polymers.[9–17] It has been known that the polaron moves as one entity consisting of both the charge and the lattice deformation with a saturation velocity after being accelerated for a short time. A breatherlike lattice oscillation is developed behind the polaron, which bears the increased energy due to the electric field acting on the polaron.[9] The polaron can move with a supersonic velocity when the electric field strengths are above 0.14 mV/Å and the maximum velocity (about four times the sound velocity) is reached at a high electric field strength ($\sim$3.5 mV/Å).[10] At even higher electric field strengths, the polaron becomes unstable and dissociates due to the charge moving faster and not allowing the distortion to occur.

Because both electron-phonon and electron-electron interactions are expected to be important features of the electronic structure of organic materials, it is necessary to address the role of these interactions on polarons. In the SSH model, however, only the electron-lattice interactions are considered while the electron-electron interactions are ignored. Therefore, it should be asked, how the electron correlation affects the dynamical properties of polymers. Many research works have suggested that the electron correlation effect is of fundamental importance for understanding the physics properties of conjugated polymers,[5] for example, the branch ratio between the singlet and the triplet excitons in

polymer-based light-emitting diodes.[18–21] The real-time dynamics of such a many-body system including both electron-phonon and electron-electron interactions is a challenging work. Fortunately, a recently developed numerical method, the adaptive time-dependent density matrix renormalization group[22] (*t*-DMRG) provides an efficient approach to perform such a task. In this paper, we apply the *t*-DMRG method on this system with both electron-phonon and electron-electron interactions, and investigate the dynamics of polarons based on the Hubbard model in weak coupling region and the *t*-*J* model in strong coupling region. The dynamical properties of the other processes, such as the recombination of oppositely charged polaron pairs and the dissociation of excitons, will be discussed elsewhere. Our results show that the effective mass is enlarged and the velocity of the polaron is suppressed by electron-electron interactions.

The paper is organized as follows: In Sec. II, we present SSH model modified to include electron-electron interactions via a Hubbard Hamiltonian for a polymer chain under the influence of an external electric field and describe the dynamical evolution method used in this work. In Sec. III the dynamical evolution of a polaron under an applied electric field will be discussed. A summary is given in Sec. IV.

II. MODEL AND METHOD

The model Hamiltonian we consider for a polymer chain in this paper takes the following form:

$$H = H_{\mathrm{el}} + H_{\mathrm{latt}} + H_E. \tag{1}$$

The first part is to describe the electron energy, which contains both the electron-lattice coupling and electron-electron interactions, modeled by Hubbard extension of an SSH-type Hamiltonian:[23–25]

$$H_{\mathrm{el}} = -\sum_{i,\sigma} t_i[c^{\dagger}_{i,\sigma}c_{i+1,\sigma} + \mathrm{H.c.}] + U\sum_i c^{\dagger}_{i\uparrow}c_{i\uparrow}c^{\dagger}_{i\downarrow}c_{i\downarrow}, \tag{2}$$

where $t_i[\equiv t_0 - \alpha(u_{i+1}-u_i)]$ is the hopping integral between sites i and $i+1$ with α the electron-lattice coupling constant and u_i the monomer displacement of site i from its undimerized equilibrium position; U is the on-site Coulomb interaction; $c^{\dagger}_{i,\sigma}(c_{i,\sigma})$ is the creation (annihilation) operator of an electron with spin σ at the site i.

The second part in Eq. (1) is to describe the lattice elastic potential energy and the kinetic energy,

$$H_{\mathrm{latt}} = \frac{K}{2}\sum_i (u_{i+1}-u_i)^2 + \frac{M}{2}\sum_i \dot{u}_i^2, \tag{3}$$

where K denotes the force constant originating from the σ bond between carbon atoms and M the mass of a site, such as that of a CH-unit for *trans*-polyacetylene.

The electric field $E(t)$ is included in the Hamiltonian as a scalar potential. This gives the following contribution to the Hamiltonian:

$$H_E = E(t)|e|\sum_i (ia + u_i)(c^{\dagger}_i c_i - 1). \tag{4}$$

The model parameters used in this work are those generally chosen for *trans*-polyacetylene: $t_0=2.5$ eV, $K=21.0$ eV/Å^2, $\alpha=4.1$ eV/Å, $a=1.22$ Å, $M=1349.14$ eV fs^2/Å^2, and a bare optical phonon energy $\hbar\omega_Q=\hbar\sqrt{4K/M}=0.16$ eV. The results are expected to be qualitatively valid for the other conjugated polymers.

Before going for the dynamical evolution, we determine the static structure of a polaron in the absence of the external electric field. The total energy is obtained by the expectation value of the Hamiltonian (1) at the ground state $|g\rangle$,

$$E_t = \langle g|H_e|g\rangle + \frac{K}{2}\sum_i (u_{i+1}-u_i)^2. \tag{5}$$

The electronic states are determined by the electronic part of the Hamiltonian (2) and the lattice configuration of the polymer $\{u_i\}$ is determined by the minimization of the total energy in the above expression

$$u_{i+1} - u_i = -\frac{\alpha}{K}\langle g|c^{\dagger}_i c_{i+1} + \mathrm{H.c.}|g\rangle + \lambda, \tag{6}$$

where λ is a Lagrangian multiplier to guarantee the polymer chain length unchanged, i.e., $\Sigma_i(u_{i+1}-u_i)=0$. The initial configuration of a polaron in the following dynamical evolution will be obtained from the solution of the above self-consistent Eq. (6) at the ground state.

At $t=0$, the polymer chain contains a positively charged polaron at the center. Then the lattice configuration at time $t(>0)$ can be obtained by the equation of motion for the atomic displacements:

$$\begin{aligned} M\ddot{u}_i(t) = &-K[2u_i(t) - u_{i+1}(t) - u_{i-1}(t)] + \alpha[\langle\psi(t)|c^{\dagger}_i c_{i+1} \\ &- c^{\dagger}_{i-1}c_i + \mathrm{H.c.}|\psi(t)\rangle] + |e|E(t)[\langle\psi(t)|c^{\dagger}_i c_i|\psi(t)\rangle - 1], \end{aligned} \tag{7}$$

where $|\psi(t)\rangle$ are the time-evolved states at time t. In principle, the time evolution can be done by operating on $|\psi(t)\rangle$ with the time-evolution operator:

$$|\psi(t+\Delta t)\rangle = e^{-iH(t)\Delta t/\hbar}|\psi(t)\rangle = e^{-i\tau H(t)}|\psi(t)\rangle. \tag{8}$$

The time development of the lattice distortions and the electronic wave functions are obtained by solving the coupled Newtonian equation of motion Eq. (7) and the time-dependent Schrödinger equation Eq. (8).

Directly solving the time-dependent Schrödinger equation for interacting many-body systems is highly nontrivial. A recently developed numerical method, the adaptive time-dependent DMRG (Ref. 22) which is an efficient implementation of Vidal's time-evolving block-decimation (TEBD) algorithm[26] in the DMRG framework,[27] enables us to perform this task. The key idea of *t*-DMRG is to incorporate the second-order Suzuki-Trotter (ST) decomposition of the time-evolution operator Eq. (8) into the DMRG finite-system algorithm. The second-order ST decomposition of the one-dimensional Hamiltonian as employed in Eq. (1) can be written as

$$e^{-i\tau H} \approx e^{-i\tau H_1/2} e^{-i\tau H_2/2} \cdots e^{-i\tau H_N/2} e^{-i\tau H_N/2} \cdots e^{-i\tau H_2/2} e^{-i\tau H_1/2} + O(\tau^3), \quad (9)$$

where H_i is the Hamiltonian of the bond i. The DMRG representation of the wave function at a particular step i during the finite-system sweep is

$$|\psi\rangle = \sum_{l\alpha_i\alpha_{i+1}r} \psi_{l\alpha_i\alpha_{i+1}r} |l\rangle |\alpha_i\rangle |\alpha_{i+1}\rangle |r\rangle, \quad (10)$$

where $|l\rangle$ and $|r\rangle$ represent the states of the left and right blocks (in a truncated basis, optimally selected as eigenvectors of a density matrix), and $|\alpha_i\rangle$ and $|\alpha_{i+1}\rangle$ represent the states of the two central sites. An operator acting on sites i and $i+1$ (only involving nearest neighbors) can be applied to $|\psi\rangle$ exactly and re-expressed in the same optimal basis as

$$[A\psi]_{l\alpha_i\alpha_{i+1}r} = \sum_{\alpha_i'\alpha_{i+1}'} A_{\alpha_i\alpha_{i+1};\alpha_i'\alpha_{i+1}'} \psi_{l\alpha_i'\alpha_{i+1}'r}. \quad (11)$$

Thus, the time-evolution operator of the bond i can be applied exactly on the DMRG step i. As a consequence, the time evolution is done by applying $e^{-i\tau H_i/2}$ at DMRG step i. Then basis transformations to the left or right are performed, until the next part of Eq. (9) can be applied. We thus apply the full operator of Eq. (9) by sweeping the site i through the system. The price to be paid is that a truncation error is introduced at each iteration step of the sweep as is known from the static DMRG. A full sweep evolves the system one time step τ. The error introduced by the second-order decomposition is order τ^3 in each time step. Thus, upon evolving the system one time unit $(1/\tau$ steps), an order τ^2 error is introduced. However, the errors mentioned can be well controlled by increasing m (the states remained per block) or decreasing τ.

The appealing feature of this algorithm is that it can be very easily implemented in existing finite-system DMRG. One uses standard finite-system DMRG to generate a high-precision initial state $|\psi(0)\rangle$ and continues to run finite-system sweeps, one for each infinitesimal time step, merely replacing the large sparse-matrix diagonalization at each step of the sweep by local bond updates for the odd and even bonds, respectively. The two main conditions for this method to be applicable, namely, that the system must be one dimensional and have only nearest-neighbor interactions, are met for the present system. In this paper, we present quasiexact numerical results of the real-time dynamics of the Hamiltonian Eq. (1) for realistic sizes of up to $N=128$ sites.

III. RESULTS AND DISCUSSIONS

In this section, we present our results on the motion of polarons in the presence of an external electric field. In our simulations, we consider a chain with total sites $N=128$. The starting geometry is obtained by minimizing the total energy of the chain where the electronic band is half filled with an extra hole. Then an electric field is turned on to accelerate the polaron. In order to reduce the lattice vibration in the accelerated process of the polaron, the electric field is turned on smoothly, that is, the field strength is increased as $E(t) = E_0 \exp[-(t-t_c)^2/t_w^2]$ for $0<t<t_c$ and $E(t)=E_0$ for $t>t_c$ with t_c being a smooth turn-on period and t_w the width. In this simulation, we take $t_w=20$ fs, $t_c=40$ fs, and $E_0=2.0$ mV/Å.

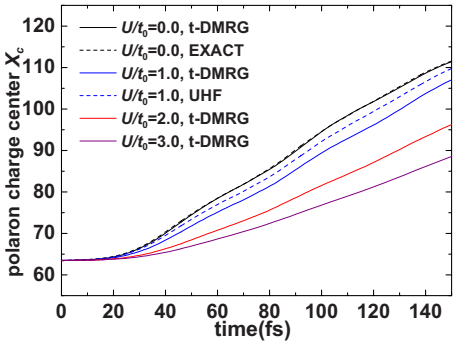

FIG. 1. (Color online) The time evolution of the charge center X_c of the polaron for different electron-electron interactions U.

The time evolution of the charge center X_c of the polaron under a moderate electric field, $E_0=2.0$ mV/Å, is shown in Fig. 1. The polaron is first accelerated, and then moves with a constant velocity as one entity consisting of both charge and lattice defects. The velocity is scaled by the sound velocity $v_s=\sqrt{4K/Ma}/2$ and is averaged in order to cancel out the fluctuations because only the saturation velocity is focused below. The stability for the polaron velocity occurs because the moving polaron shall emit localized phonons, multibreather excitations, which bear the increased energy of the system due to the external electric field.[9]

From Fig. 1, the following issues should be addressed: First, in order to confirm the validity of our results, we compare the t-DMRG calculations (keeping $m=200$ states per block and using a time step $\tau=0.1$) with the exact numerical results for a noninteracting $(U=0)$ chain of the same set of parameters described above. The excellent agreement was found in both the charge center X_c and the staggered bond parameters up to $t\sim 180$ fs. Second, the polaron velocity is decreased with increasing the Coulomb interaction U. At last, one can find that the polaron velocity calculated by the t-DMRG is smaller than that obtained at the UHF level. The electron correlation effects have been considered in t-DMRG calculations, thus, it indicates that the motion of polarons is more suppressed by the electron correlation effects. Moreover, it should be noted that the polaron velocity depends not only on the electron-electron interaction, but also on the electron-phonon coupling constant, the sound velocity, etc. In what follows, in order to study the electron correlation effects on the polaron dynamics, we will only focus on the saturation velocities of the polaron for different electron-electron interaction strengths with the condition that the other parameters are fixed.

A. In the weak coupling region

As described above, the motion of a charged polaron has been presented in the weak coupling region $(U/t_0 \leq 3.0)$, based on the SSH and Hubbard model. Figure 2 shows that the saturation velocity of a polaron varies with the on-site

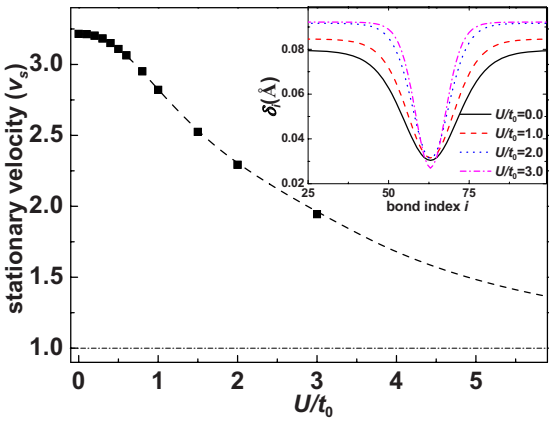

FIG. 2. (Color online) The saturation velocity of a polaron driven by an external electric field (E_0=2.0 mV/Å) as a function of U. The inset shows the staggered bond order parameter δ_i of a static polaron for several values of U in Hubbard model. The dash line is given as a guide to the eye, and the dash-dot line correspond to the $U=\infty$ limit, the sound velocity of the system (see text).

Coulomb interaction U. One can find that the Coulomb repulsion restrains the motion of the polaron and the saturation velocity of the polaron reaches its maximum value at $U=0$. This can be understood as that the electron localized in the polaron has to overcome the potential barrier induced by Hubbard U in order to move from one site to another because the lattice tends to be singly occupied in the spin-density-wave (SDW) phase.

For further understanding of the electron correlation effects on the polaron velocity, we explore the relation between the saturation velocity of the polaron and its localization from a static view. The staggered bond order parameter $\delta_i = (-1)^i(2u_i - u_{i-1} - u_{i+1})/4$ of a static polaron is shown in the inset of Fig. 2 for several values of U. It is found that the width of the polaron is a decreasing function of the Hubbard U. The narrower the width is, the stronger effective potential the localized charge in the polaron feels. As a result, the binding energy is increased, which leads to the localization of the polaron is enhanced by the Coulomb repulsion, and the polaron stability increases. Along with the increase of the binding energy, the effective mass of the polaron is enlarged, thus the saturation velocity of the polaron decreases. It should be stressed that a similar tendency has been observed at the UHF level,[14] but the detailed physical origin is substantially different from the DMRG results. At the UHF level, only the enhanced localization of the polaron is found, the dimerization of the polymer chain is less affected by the on-site Coulomb interaction U, see the inset of Fig. 3 in Ref. 12. In contrast, the enhanced dimerization is observed in the weak coupling region from the DMRG results, see the inset of Fig. 2, which arises from the electron correlation effects.[28] The enhanced dimerization will decrease the polaron velocity furthermore.

In connection with the saturation of the velocity, it is interesting to trace the behavior of the effective mass of polarons. The static lattice configuration is smoothed by spline interpolation, allowing us to compute the configuration at any desired points. Then, the polaron effective mass can be

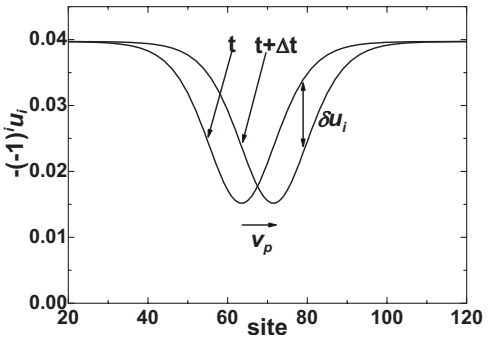

FIG. 3. Schematic picture of the time dependence of the bond order parameter for a polaron-containing chain.

determined by calculating the energy of a slowly moving domain wall

$$u(x,t) = u(x - v_p t, t). \tag{12}$$

The schematic representation of the time dependence of the polaron configuration is illustrated in Fig. 3. Using the adiabatic approximation for the electronic motion, one can show that the effective mass of the polaron is related δu_i for a small change in domain wall position by

$$\frac{1}{2}\sum_i M\dot{u}_i^2(t) = \frac{1}{2}m_p v_p^2. \tag{13}$$

It is clear that the effective mass will appear in the transport coefficients of the polaron.

In Fig. 4, the U dependence of the effective mass m_p scaled by the free electron mass m_e is summarized.[29] As stated above, one can find that the effective mass increases with increasing repulsive interaction. The increase of effective mass is consistent with the fact that the repulsive interaction makes the polaron width narrower. In general, the narrower is the width of a polaron, the larger is its effective mass, as similar as that of a soliton.[1] With the polaron effective mass increasing, its velocity decreases.

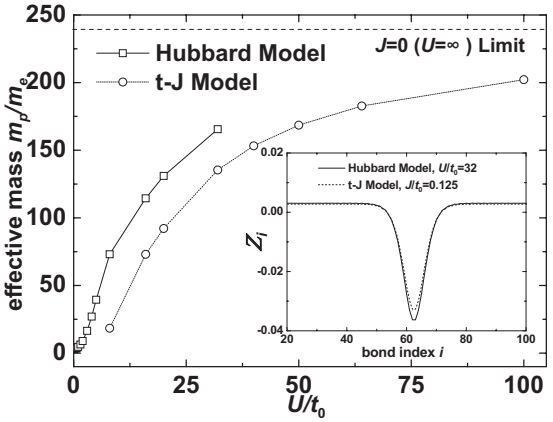

FIG. 4. The U dependence of the polaron effective mass m_p scaled by the free electron mass m_e. The square lines are for the Hubbard model results and the circles lines for the t-J model results. The inset shows the acoustical order parameter Z_i calculated in the Hubbard model and the t-J model, respectively.

B. In the strong coupling region

Next, let us discuss the polaron dynamical properties in the strong coupling region. When the Coulomb interaction U is too large, some difficulties, such as slower convergence and worse precision, are encountered numerically. Moreover, the polaron takes long time to reach the saturation velocity, such that eventually the adaptive t-DMRG will break down. Therefore, it is difficult to calculate the saturation velocity of the polaron by the t-DMRG method directly in the case of the Hubbard U tending to infinity. Instead, we investigate the polaron velocity from its effective mass point of view. In the limit $U/t_0 \gg 1$, double occupancy $|\uparrow\downarrow\rangle$ can be excluded, this results in the t-J model

$$H_{t\text{-}J} = -\sum_{i,\sigma} t_i[\tilde{c}^{\dagger}_{i,\sigma}\tilde{c}_{i+1,\sigma} + \text{H.c.}] + \sum_i J_i\left(\vec{S}_i\vec{S}_{i+1} - \frac{1}{4}n_i n_{i+1}\right), \tag{14}$$

where $\tilde{c}_{i\sigma}=(1-n_{i-\sigma})c_{i\sigma}$ (here $n_{i\sigma}=c^{\dagger}_{i\sigma}c_{i\sigma}$), $\vec{S}_i = 1/2\Sigma_{\alpha\beta}c^{\dagger}_{i\alpha}(\vec{\sigma})_{\alpha\beta}c_{i\beta}$, and $n_i=\Sigma_\sigma n_{i\sigma}$, in which the spin-spin interaction $J_i=4t_i^2/U$ is due to a second-order virtual hopping process possible only for electrons of opposite spin on sites i and $i+1$.

The static lattice configuration of the polaron can be obtained by solving self-consistently the following equations:

$$u_{i+1} - u_i = t_0\frac{2\alpha J\langle S_{i,i+1}\rangle - \alpha\langle B_{i,i+1}\rangle - \lambda}{t_0 K + 2J\alpha^2\langle S_{i,i+1}\rangle}, \tag{15}$$

in which the Lagrangian multiplier λ satisfies:

$$\lambda\sum_i \frac{1}{t_0 K + 2J\alpha^2\langle S_{i,i+1}\rangle} = \sum_i \frac{2\alpha J\langle S_{i,i+1}\rangle - \alpha\langle B_{i,i+1}\rangle}{t_0 K + 2J\alpha^2\langle S_{i,i+1}\rangle}. \tag{16}$$

Where $J \equiv 4t_0/U$; $\langle B_{i,i+1}\rangle = \Sigma_\sigma\langle g|\tilde{c}^{\dagger}_{i\sigma}\tilde{c}_{i+1\sigma} + \text{H.c.}|g\rangle$ and $\langle S_{i,i+1}\rangle = \langle g|\vec{S}_i\vec{S}_{i+1} - \frac{1}{4}n_i n_{i+1}|g\rangle$ are the bond-correlation and spin-correlation functions, respectively. In the inset of Fig. 4, we present a comparison of the polaron conformations obtained from the Hubbard model and the t-J model at $U/t_0 = 32$. It is clearly shown that the bond order parameter of the Hubbard model is almost the same as that of the t-J model.

Then, the effective mass m_p of the polaron can be calculated by using the same method described above. The U dependence of the effective mass m_p calculated in the t-J model is also plotted in Fig. 4. A similar tendency as that in Hubbard model, i.e., the effective mass increases with increasing repulsive interaction, is clearly seen, although the polaron effective mass calculated by the t-J model is smaller than that obtained by the Hubbard model. At $U=\infty$ limit, the second term in Eq. (14) vanishes, so Eq. (14) reduces to a single-particle problem. Moreover, all the energy levels are occupied by $1/\sqrt{2}(|\uparrow\rangle + |\downarrow\rangle)$ except for the highest energy level. Then the t-J Hamiltonian can be mapped onto an acoustic polaron model due to the particle-hole symmetry. It has been known that the saturation velocity of an acoustic polaron is the sound velocity of the system.[30] Also, the saturation velocity of the acoustic polaron has been estimated from the time dependence of the velocity, which is slightly smaller than the sound velocity.[31] From the staggered bond order parameter of the acoustic polaron, we obtain its effective mass $m_\infty \simeq 240\, m_e$ (the dash line in Fig. 4), which is rather heavier than the effective mass of the optical polaron at $U=0$ (about 3.3 m_e).

Finally, it should be stated that we obtain the effective mass from the static geometry structure of the polaron and assume that the geometry does not change when it moves. In fact, the moving polaron shall emit phonons to keep its steady motion,[9] and the width of a moving polaron shows small oscillations in time because of the excitation of amplitude modes. Therefore, the effective mass of the polaron obtained in this paper may be slightly different from that of a moving polaron.

IV. SUMMARY

In summary, the effects of electron-electron interaction on the motion of a polaron driven by an external electric field in conjugated polymers are investigated by using an adaptive t-DMRG method, based on the SSH model and the Hubbard model. It has been shown that the t-DMRG is an efficient approach to perform a real-time dynamics of many-body systems including both electron-electron and electron-phonon interactions. Our results show that the motion of the polaron is suppressed by the on-site Coulomb interaction U. The effective mass of the polaron is enlarged and the saturation velocity of the polaron decreases monotonically with the on-site repulsions. Additionally, the saturation velocity of the polaron reaches the minimum value, the sound velocity, when the Coulomb interaction U tends to infinite.

ACKNOWLEDGMENTS

This work was supported by National Natural Science Foundation of China, the MSTC of China (Contract No. 2006CB921302), the EC Project OFSPIN (Contract No. NMP3-CT-2006-033370), and Program for New Century Excellent Talents in University (NCET).

[1] A. J. Heeger, S. Kivelson, J. R. Schrieffer, and W. P. Su, Rev. Mod. Phys. **60**, 781 (1988).

[2] M. Kertész and P. R. Surján, Solid State Commun. **39**, 611 (1981).

[3] W. P. Su, J. R. Schrieffer, and A. J. Heeger, Phys. Rev. Lett. **42**, 1698 (1979); Phys. Rev. B **22**, 2099 (1980).

[4] S. A. Brazovskii and N. N. Kirova, Sov. Phys. JETP **33**, 4 (1981).

[5] *Primary Photoexcitations in Conjugated Polymers: Molecular Exciton Versus Semiconductor Band Model*, edited by N. S. Sar-

iciftci (World Scientific, Singapore, 1997), and references therein.
[6] I. H. Campbell and D. L. Smith, Solid State Phys. **55**, 1 (2001), and references therein.
[7] Z. An, C. Q. Wu, and X. Sun, Phys. Rev. Lett. **93**, 216407 (2004).
[8] A. Nitzan and M. A. Ratner, Science **300**, 1384 (2003).
[9] J. F. Yu, C. Q. Wu, X. Sun, and K. Nasu, Phys. Rev. B **70**, 064303 (2004).
[10] A. A. Johansson and S. Stafström, Phys. Rev. Lett. **86**, 3602 (2001); Phys. Rev. B **69**, 235205 (2004).
[11] S. V. Rakhmanova and E. M. Conwell, Appl. Phys. Lett. **75**, 1518 (1999).
[12] C. Q. Wu, Y. Qiu, Z. An, and K. Nasu, Phys. Rev. B **68**, 125416 (2003).
[13] Y. H. Yan, Z. An, and C. Q. Wu, Eur. Phys. J. B **42**, 157 (2004).
[14] B. Di, Z. An, Y. C. Li, and C. Q. Wu, Europhys. Lett. **79**, 17002 (2007).
[15] Z. An, B. Di, H. Zhao, and C. Q. Wu, Eur. Phys. J. B **63**, 71 (2008).
[16] Y. Ono and A. Terai, J. Phys. Soc. Jpn. **59**, 2893 (1990).
[17] X. Liu, K. Gao, J. Fu, Y. Li, J. Wei, and S. Xie, Phys. Rev. B **74**, 172301 (2006).
[18] Z. Shuai, D. Beljonne, R. J. Silbey, and J. L. Bredas, Phys. Rev. Lett. **84**, 131 (2000).
[19] D. Beljonne, A. Ye, Z. Shuai, and J. L. Brédas, Adv. Funct. Mater. **14**, 684 (2004).
[20] M. Wohlgenannt, K. Tandon, S. Mazumdar, S. Ramasesha, and Z. V. Vardeny, Nature (London) **409**, 494 (2001).
[21] M. Wohlgenannt, C. Yang, and Z. V. Vardeny, Phys. Rev. B **66**, 241201(R) (2002).
[22] S. R. White and A. E. Feiguin, Phys. Rev. Lett. **93**, 076401 (2004).
[23] P. R. Surján, L. Udvardi, and K. Németh, J. Mol. Struct.: THEOCHEM **311**, 55 (1994).
[24] P. R. Surján, A. Lázár, and M. Kállay, Phys. Rev. B **58**, 3490 (1998).
[25] S. Mazumdar and S. N. Dixit, Phys. Rev. Lett. **51**, 292 (1983).
[26] G. Vidal, Phys. Rev. Lett. **93**, 040502 (2004).
[27] S. R. White, Phys. Rev. Lett. **69**, 2863 (1992); U. Schollwöck, Rev. Mod. Phys. **77**, 259 (2005).
[28] C. Q. Wu, X. Sun, and K. Nasu, Phys. Rev. Lett. **59**, 831 (1987).
[29] The results of the analytic calculations, which are valid in the absence of U; the soliton effective mass is about $6m_e$ (Ref. 3). The result of our numerical method for the case of soliton yields $m_s \simeq 6.02m_e$, which is consistent with the analytic result.
[30] E. G. Wilson, J. Phys. C **16**, 6739 (1983).
[31] Y. Arikabe, M. Kuwabara, and Y. Ono, J. Phys. Soc. Jpn. **65**, 1317 (1996).